nature chemistry

ARTICLES

https://doi.org/10.1038/s41557-019-0398-3

Global aromaticity at the nanoscale

Michel Rickhaus[1,3,4], Michael Jirasek[1,4], Lara Tejerina[1], Henrik Gotfredsen[1], Martin D. Peeks[1,2], Renée Haver[1], Hua-Wei Jiang[1], Timothy D. W. Claridge[1] and Harry L. Anderson[1*]

Aromaticity can be defined by the ability of a molecule to sustain a ring current when placed in a magnetic field. Hückel's rule states that molecular rings with [4*n* + 2] π-electrons are aromatic, with an induced magnetization that opposes the external field inside the ring, whereas those with 4*n* π-electrons are antiaromatic, with the opposite magnetization. This rule reliably predicts the behaviour of small molecules, typically with fewer than 22 π-electrons (*n* = 5). It is not clear whether aromaticity has a size limit, or whether Hückel's rule extends to much larger macrocycles. Here, we present evidence for global aromaticity in porphyrin nanorings with circuits of up to 162 π-electrons (*n* = 40); aromaticity is controlled by changing the constitution, oxidation state and conformation. Whenever a ring current is observed, its direction is correctly predicted by Hückel's rule. The largest ring currents occur when the porphyrin units have fractional oxidation states.

The extent of electronic delocalization in linear molecules is limited by the onset of symmetry-breaking transitions, which can be viewed as Peierls-type electron–vibration interactions or as shifts in mixed-valence behaviour[1]. For example, cyanine dyes feature a linear chain of C–C bonds with bond order 1.5 and negligible bond length alternation (like the C–C bonds in benzene) resulting in charge delocalization, but if the chain exceeds a critical length, the symmetry collapses, localizing the charge[2,3]. It is not clear whether similar effects limit the size of an aromatic ring, or whether molecular ring currents can extend into the domain of mesoscopic phenomena such as Aharonov–Bohm oscillations[4]. Many new globally aromatic macrocycles have been reported during the last few years[5–18], but apart from the porphyrin nanorings discussed here, there are no reports of aromatic rings with more than 62 π-electrons[7].

Here we explore circuits of up to 162 π-electrons in a large family of nanorings in a wide range of oxidation states. In these nanorings, each porphyrin contributes ten electrons to the Hückel π-electron count, and each linking alkyne contributes two electrons, so a nanoring cation ***c*-P*N*[$\mathbf{b}_x\mathbf{e}_y$]$^{Q+}$** has an electron count of $10N + 4x + 2y - Q$ (where N is the number of porphyrin units, x and y are the number of butadiyne and ethyne links, respectively, and Q is the oxidation state). Recently, we reported that the butadiyne-linked six-porphyrin nanoring ***c*-P6[$\mathbf{b}_6$]** displays global aromaticity when oxidized[8], reduced[17] or electronically excited[18]. According to Schleyer's terminology[19], all the nanorings discussed here are 'trannulenes' rather than 'annulenes', because the *p* orbitals making up the aromatic π-system are oriented in the plane of the ring, whereas in annulenes the *p* orbitals are perpendicular to the ring. Trannulenes follow Hückel's rule in the same way as annulenes, although Hückel did not anticipate this type of system[20].

Results and discussion

The six-porphyrin nanoring complexes ***c*-P6[$\mathbf{e}_6$]·T6***, ***c*-P6[$\mathbf{be}_5$]·T6***, ***c*-P6[$\mathbf{b}_5\mathbf{e}$]·T6** and ***c*-P6[$\mathbf{b}_6$]·T6** provide a homologous series of compounds in which we systematically vary the number of π-electrons by changing the number of -C≡C- units while preserving the circular geometry[21,22] (which is locked by the template, **T6*** or **T6**, six-legged structures with a central benzene and 4-pyridyl legs; Fig. 1). The ^{1}H NMR spectra of all four complexes were recorded in the 2+, 4+ and 6+ oxidation states, revealing the presence of aromatic or antiaromatic ring currents. The directions of these ring currents agree perfectly with Hückel's rule. Thus, ***c*-P6[$\mathbf{e}_6$]·T6*** (neutral: 72 π-electrons) and ***c*-P6[$\mathbf{b}_6$]·T6** (neutral: 84 π-electrons) are both aromatic in the 2+ and 6+ oxidation states and antiaromatic in the 4+ state, whereas ***c*-P6[$\mathbf{be}_5$]·T6*** (neutral: 74 π-electrons) and ***c*-P6[$\mathbf{b}_5\mathbf{e}$]·T6** (neutral: 82 π-electrons) are both antiaromatic in the 2+ and 6+ states and aromatic in the 4+ state.

The most obvious evidence for these ring currents comes from the chemical shifts of the template α- and β-pyridyl ^{1}H resonances; for example, these protons are strongly shielded ($\delta_H = -7.3$ and −3.6 ppm vs 8.7 and 7.5 ppm, respectively, in the free template) in aromatic ***c*-P6[$\mathbf{e}_6$]·T6*$^{2+}$** and strongly deshielded ($\delta_H = 36.0$ and 30.1 ppm, respectively) in antiaromatic ***c*-P6[$\mathbf{e}_6$]·T6*$^{4+}$**. Further evidence is provided by the ^{1}H and ^{13}C signals of the trihexylsilyl (THS) groups in the porphyrins. In each spectrum, we observe one group of THS signals at 0–2 ppm that is essentially unshifted compared with the signals of the neutral compounds (peaks coloured orange in Fig. 1), which arise from the external THS groups located near the zero-shielding cone of the nanoring (THS_{out}, Fig. 2), and one group of THS signals that is shielded or deshielded depending on the direction of the ring current (THS_{in}, coloured green in Figs. 1 and 2). Interconversion of THS_{in} and THS_{out} is slow on the NMR timescale, and the assignment of the THS_{in} signals is confirmed by the observation of nuclear Overhauser effects (NOEs) to protons of the template (**T6** or **T6***). There is an excellent linear correlation between the changes in the chemical shift of the α-pyridyl template ^{1}H and ^{13}C signals and the THS CH_2-Si and CH_3 ^{1}H and ^{13}C signals, showing that all six signals report on the same global ring currents (Supplementary Figs. 70–73).

The observed ring currents in this set of 12 species (four nanorings in three oxidation states) were compared with the results of nucleus-independent chemical shift (NICS) calculations[23,24]. We screened a range of density functional theory (DFT) functionals for these NICS calculations (see Supplementary Figs. 80 and 83). The B3LYP functional[25] gave good agreement with the NMR results for most species, but it failed to reproduce the antiaromaticity of the dications ***c*-P6[$\mathbf{be}_5$]$^{2+}$** and ***c*-P6[$\mathbf{b}_5\mathbf{e}$]$^{2+}$**. The LC-ωhPBE

[1]Department of Chemistry, University of Oxford, Oxford, UK. [2]School of Chemistry, University of New South Wales, Sydney, New South Wales, Australia. [3]Present address: Department of Chemistry, University of Zurich, Zurich, Switzerland. [4]These authors contributed equally: Michel Rickhaus, Michael Jirasek. *e-mail: harry.anderson@chem.ox.ac.uk

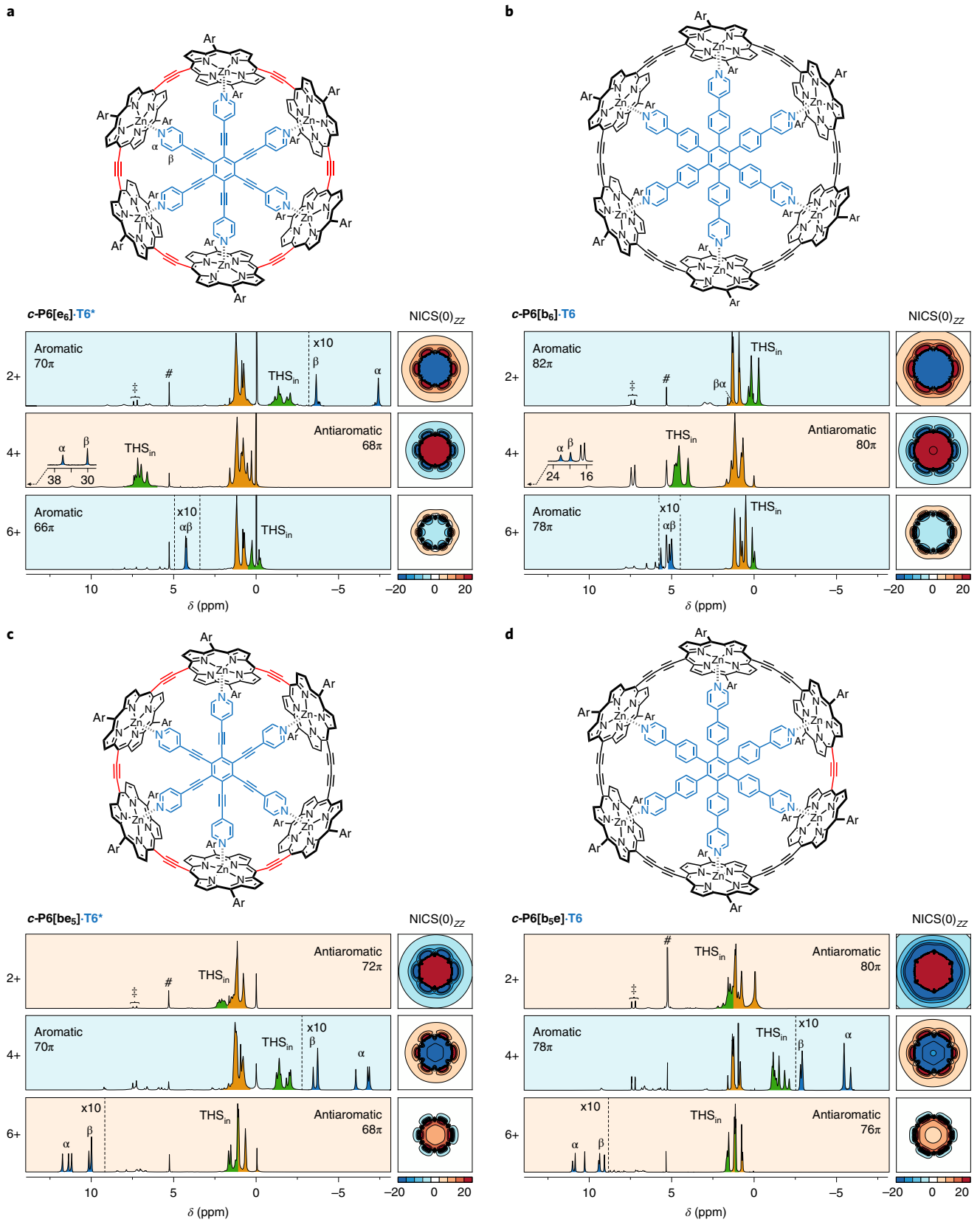

Fig. 1 | ^{1}H NMR spectra of the aromatic and antiaromatic six-porphyrin nanoring template complexes in oxidation states 2+, 4+ and 6+. **a**, ***c*-P6[e$_6$]·T6***. **b**, ***c*-P6[b$_6$]·T6**. **c**, ***c*-P6[be$_5$]·T6***. **d**, ***c*-P6[b$_5$e]·T6**. Ar, 3,5-bis(trihexylsilyl)phenyl. The ^{1}H NMR spectra were recorded at 500 MHz in CD_2Cl_2. The oxidized states were generated by titration with thianthrenium hexafluoroantimonate. The symbols # and ‡ denote $CHDCl_2$ and thianthrene signals, respectively. Detailed spectra are shown in Supplementary Figs. 9–12 and 19–34. Dashed vertical lines indicate tenfold magnifications. A grid plot of the NICS(0)$_{zz}$ value in the *xy* plane of the nanoring, calculated without the template, is shown for each oxidation state of each complex (5 × 5 nm; LC-ωhPBE/6-31G*, $\omega = 0.1$; the colour axis is truncated above 20 and below −20 ppm; contours are drawn every 5 ppm).

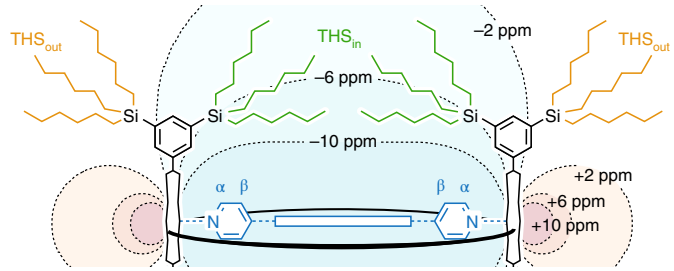

Fig. 2 | Magnetic shielding plotted in the *xz* plane perpendicular to the plane of the nanoring. NICS$_{iso}$ contours for ***c*-P6[e$_6$]·T6*$^{2+}$** are shown from –10 to 10 ppm. Internal trihexylsilyl groups (THS$_{in}$, green) are sensitive to the global ring current, whereas external ones (THS$_{out}$, orange-brown) are not.

($\omega = 0.1$) functional[26] gave the best agreement with the observed NMR shifts (see plots on the right of each spectrum in Fig. 1) and we chose this functional for all the NICS calculations shown in this article.

The evolution of the ring current with increasing ring size is illustrated by the ^{1}H NMR spectra of the eight-porphyrin nanoring complex ***c*-P8[e$_8$]·(T4*)$_2$**, which has a circuit of 96 π-electrons when neutral[21] (Fig. 3). The THS and template protons show clear evidence for aromaticity in the 2+ and 6+ oxidation states, whereas the 4+ and 8+ oxidation states are antiaromatic. These results match the predictions of Hückel's rule and agree with the calculated NICS values (Fig. 3). The magnitude of the ring current varies substantially between the different oxidation states; thus, the mean change in the chemical shift of the α-pyridyl protons of the template

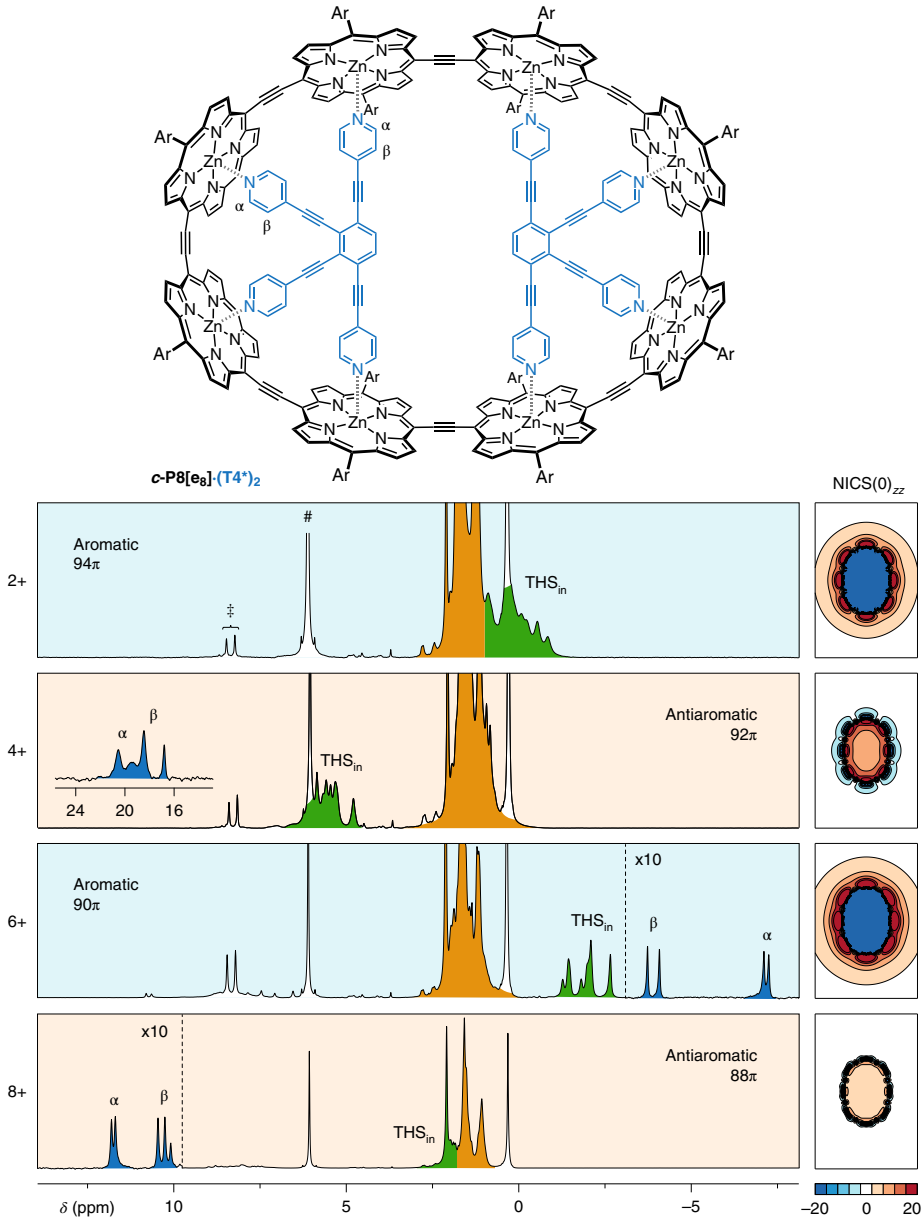

Fig. 3 | Hückel behaviour in a template-bound eight-porphyrin ring. Molecular structure of ***c*-P8[e$_8$]·(T4*)$_2$** (Ar, 3,5-bis(trihexylsilyl)phenyl; each porphyrin unit has two Ar substituents, but in some cases one of them is hidden by the template) and its ^{1}H NMR spectra in the oxidation states 2+, 4+, 6+ and 8+. The key resonances of THS$_{in}$ (green), THS$_{out}$ (orange) and the template (α, β) are shown; # and ‡ denote $CHDCl_2$ and thianthrene signals, respectively. Detailed spectra are shown in Supplementary Figs. 14 and 45–47. NICS(0)$_{zz}$ grids (LC-ωhPBE/6-31G*, $\omega = 0.1$) in the *xy* plane are shown for each state (without the template).

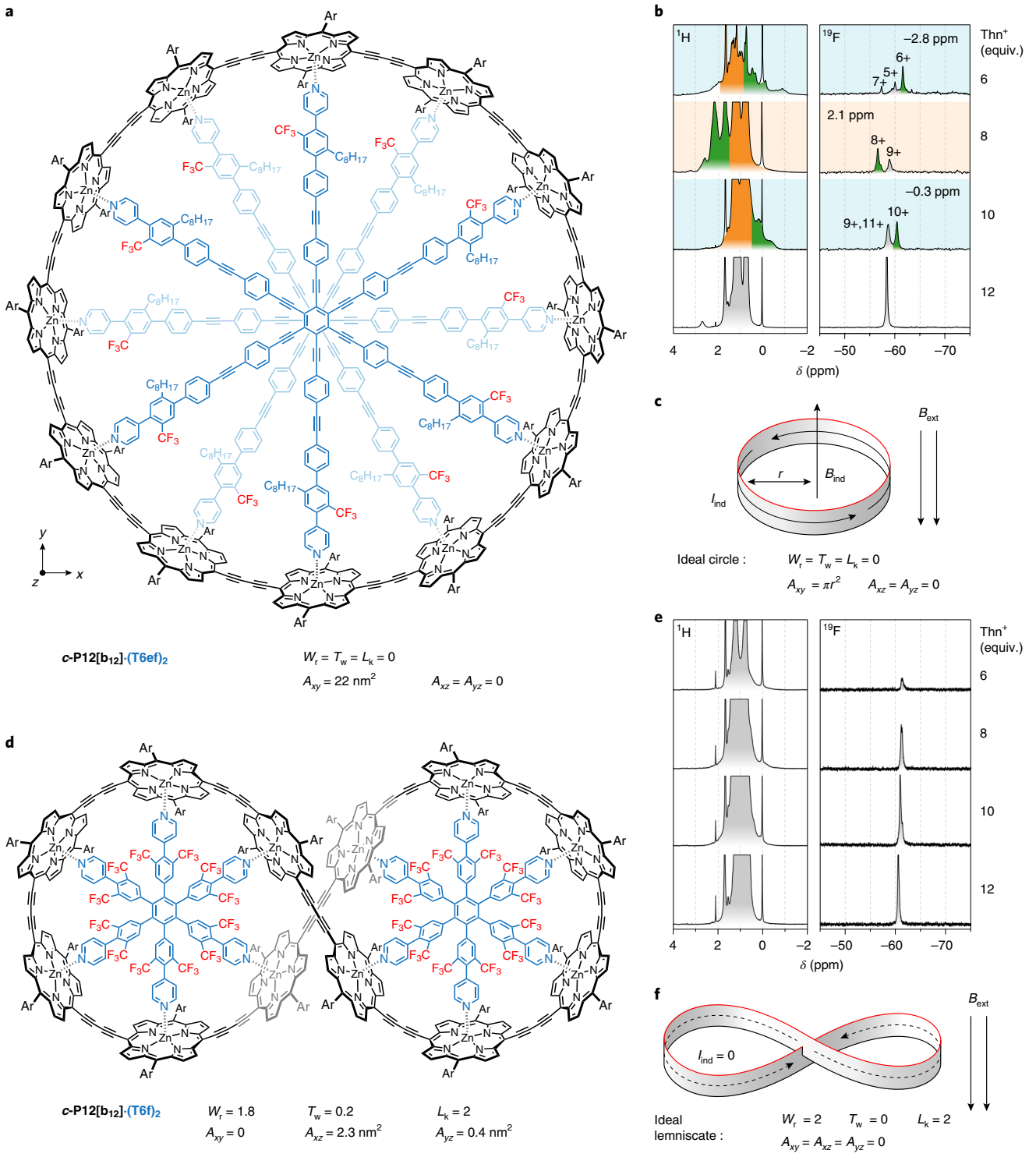

Fig. 4 | Ring currents in topologically distinct 12-porphyrin ring complexes. a, Molecular structure of **c-P12[b_{12}]·(T6ef)$_2$** with two stacked bound template units. **b**, ^{1}H and ^{19}F NMR spectra of oxidized **c-P12[b_{12}]·(T6ef)$_2$**. Ar, 3,5-bis(trihexylsilyl)phenyl. Green shading indicates the interior THS_{in} resonances and orange shading the external THS_{out} resonances; background colours indicate a global aromatic (blue) or antiaromatic (orange) state. Thn$^+$, thianthrenium. **c**, A circular conformation is predicted to exhibit a ring current and thus an induced magnetic moment in an external magnetic field. B_{ext}, external magnetic field; B_{ind}, induced magnetic field; I_{ind}, induced current; *r*, radius. **d**, Molecular structure of the **c-P12[b_{12}]·(T6f)$_2$** figure-of-eight complex. **e**, ^{1}H and ^{19}F NMR spectra of oxidized **c-P12[b_{12}]·(T6f)$_2$**. **f**, In the lemniscate, the two loops induce opposite currents that cancel, and no ring current is expected. Detailed spectra are shown in Supplementary Figs. 17, 18 and 58–67. For **c-P12[b_{12}]·(T6f)$_2$**, $A_{xy}=0$ because the lemniscate has D_2 symmetry and the areas of the two loops cancel.

(relative to unbound **T4***, $\delta_\alpha = 8.67$ ppm) is $\Delta\delta_\alpha = +11.8$ ppm in the 4+ state and −15.6 ppm in the 6+ state, but it dwindles to +1.9 ppm in the 8+ state.

Fluorinated templates allow the aromaticity of nanorings to be evaluated using ^{19}F NMR titrations, as exemplified by the extended six-legged template **T6ef** (Fig. 4a). Two molecules of this template

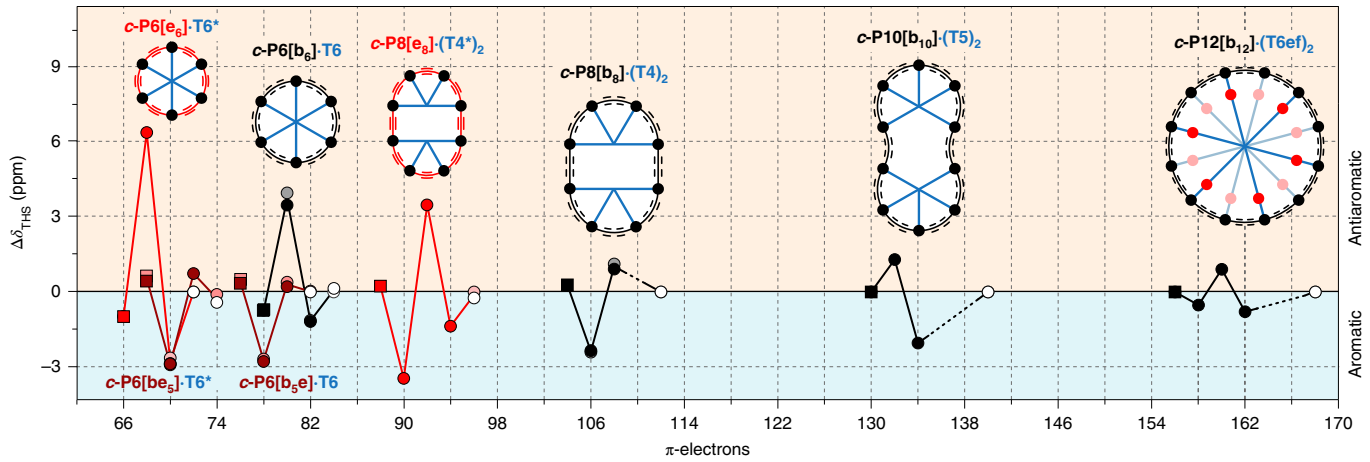

Fig. 5 | Summary of the shielding and deshielding of the trihexylsilyl groups across eight different nanorings. Schematic representation of related porphyrin rings. Red indicates ethyne links, black indicates butadiyne links, black dots indicate zinc porphyrins and templates are shown in blue. Plot of the observed ^{1}H chemical shift difference between the inner and outer THS protons, $\Delta\delta_{THS} = \delta_{THSin} - \delta_{THSout}$, for each oxidation state of the nanoring. Positive or negative shifts indicate a global antiaromatic or aromatic current, respectively. Empty circles indicate neutral rings ($\Delta\delta_{THS} = 0$) and squares indicate oxidation states with $P_{OX} = 1$. Vertical dashed lines denote oxidation states with $4n + 2$ π-electrons. The lines connecting the points are for visual guidance only. $\Delta\delta_{THS}$ is plotted for the CH_3 (dark points) and $SiCH_2$ signals (faded points) of the THS chains.

stack to form a stable 2:1 complex with a 12-porphyrin nanoring, ***c*-P12[b$_{12}$]·(T6ef)$_2$** (circuit electron count: 168 π-electrons when neutral[27]) in which the CF_3 groups are positioned to probe the global ring current. The CF_3 ^{19}F resonance is shielded in the aromatic 6+ and 10+ oxidation states, but deshielded in the antiaromatic 8+ oxidation state (Fig. 4b). The shifts of the CF_3 ^{19}F resonance are fully consistent with the shifts of the THS_{in} ^{1}H signals (shaded green, Fig. 4b) and they agree with the predictions of NICS calculations. A range of DFT functionals were tested for ***c*-P12[b$_{12}$]$^{Q+}$** and, as for the six-porphyrin rings, LC-ωhPBE ($\omega = 0.1$) was found to give the best agreement with the experimental ring current shifts (see Supplementary Figs. 88–90 and Supplementary Tables 7 and 8).

No aromatic or antiaromatic ring current was detected for the 12+ oxidation state, and this result is reproduced by the NICS calculations, although this 12+ state is expected to be antiaromatic (156 π-electrons; $4n$, $n = 39$). The ^{19}F NMR titrations also show CF_3 signals attributed to the open-shell 5+, 7+, 9+ and 11+ oxidation states, at similar chemical shifts to the neutral compound; thus, the shielding or deshielding effects in the open-shell cations are small compared with those in closed-shell species. Exchange spectroscopy (EXSY) NMR experiments show that the odd-electron oxidation states are in chemical exchange with the even-electron states on a timescale of seconds. It is not surprising that mixtures of oxidation states are formed during these titrations, because the oxidation potentials are closely spaced (for calculated speciation curves, see Supplementary Fig. 79), but it is remarkable that these open-shell species give spectra that are sharp enough to be observed.

We used the 12-porphyrin nanoring ***c*-P12[b$_{12}$]** to explore the relationship between the three-dimensional conformation and aromaticity. The magnitude of the ring current induced in a macroscopic ring of metal wire depends on the total magnetic flux passing through the ring. If the ring has a figure-of-eight shape, with two equal lobes such that the magnetic flux passing through each loop induces equal and opposite currents, then there will be no net ring current. We sought to test whether this principle applies on the molecular scale, so we synthesized a small six-legged template, **T6f**, which forms a figure-of-eight-shaped[27] 1:2 complex, ***c*-P12[b$_{12}$]·(T6f)$_2$** (which is doubly twisted, not Möbius[28,29], Fig. 4d), and investigated the ring currents in this system by ^{1}H and ^{19}F NMR spectroscopy as a function of oxidation state under identical conditions to those used for the circular ***c*-P12[b$_{12}$]·(T6ef)$_2$**. The resulting ^{1}H, ^{13}C and ^{19}F NMR spectra show the absence of any detectable ring currents ($\Delta\delta < 0.1$ ppm) in the figure-of-eight nanoring, confirming that aromaticity can be switched on and off by geometry (Fig. 4e). This result is reproduced by the NICS calculations (Supplementary Fig. 91).

The suppression of ring currents in figure-of-eight-shaped annulenes has been predicted theoretically[28,30], but it has not been observed experimentally in other figure-of-eight-shaped aromatic systems[6,7,14,28,29,31], probably because they were not the right shape to achieve cancellation of the ring current. The topology of a closed ribbon can be described by the linking number L_k, the writhe W_r and the twist T_w (refs. [32–34]). Total cancellation of the ring current is expected for an ideal lemniscate geometry with $W_r = 2$, $T_w = 0$ and $L_k = 2$ with D_2 symmetry[28] (Fig. 4f), which is close to the geometry of ***c*-P12[b$_{12}$]·(T6f)$_2$** ($W_r = 1.8$, $T_w = 0.2$ and $L_k = 2$, from the crystal structure of ***c*-P12[b$_{12}$]·(T6)$_2$**; ref. [35]). The ***c*-P12[b$_{12}$]·(T6ef)$_2$** ring has a large cross-sectional area ($A_{xy} = 22\,nm^2$; $A_{xz} = A_{yz} = 0$; Fig. 4c) resulting in a substantial ring current, whereas the ***c*-P12[b$_{12}$]·(T6f)$_2$** lemniscate has a small net cross-sectional area ($A_{xy} = 0$, $A_{xz} = 2.3\,nm^2$, $A_{yz} = 0.4\,nm^2$; Supplementary Fig. 93) resulting in a weak response to magnetic field. The ring current in ***c*-P12[b$_{12}$]·(T6f)$_2$** is blocked by the global topology ($T_w \approx 0$ and $W_r \approx 2$), not by any local break in π-conjugation.

The ring currents observed in this whole family of nanorings are summarized in Fig. 5, which shows the shift in the THS_{in} resonances ($\Delta\delta_{THSin}$) as a function of oxidation state. Whenever a ring current is observed, its direction (aromatic or antiaromatic) matches the prediction from Hückel's rule. The magnitude of the ring current varies with the average oxidation state of the porphyrin units ($P_{OX} = Q/N$). The largest ring currents are observed in mixed-valence systems, where $P_{OX} \approx +0.5$ to $+0.7$. Global ring currents are not observed in the neutral rings ($P_{OX} = 0$), in which the local porphyrin ring current dominates; in the larger rings, the ring current also almost vanishes when $P_{OX} = 1$ (see square points for ***c*-P8[b$_8$]·(T4)$_2$$^{8+}$**, ***c*-P10[b$_{10}$]·(T5)$_2$$^{10+}$** and ***c*-P12[b$_{12}$]·(T6ef)$_2$$^{12+}$** in Fig. 5). The formation of a mixed-valence state appears to be essential for efficient nanoscale charge delocalization, just as the presence of a partially filled band is essential for conductance in an extended lattice[36].

Hückel's rule was originally formulated to explain the unusual properties of benzene and other molecules with six π-electrons[37]. It is remarkable that this simple rule correctly predicts the magnetic response of large oxidized nanorings with circuits of up to 162 π-electrons. This work shows that electronic delocalization can extend coherently around molecular rings with circumferences of 16 nm. These supramolecular rings allow the magnitude of the ring current to be controlled by topology in a way that has not yet been demonstrated for small molecules.

Methods

All ^{1}H NMR oxidation titrations were carried out by adding a well-stirred suspension of thianthrenium hexafluoroantimonate to a solution of the porphyrin nanoring in CD_2Cl_2 at −60 to −20 °C under a counterflow of argon (see Supplementary Information for details). These oxidation experiments were conducted in NMR tubes fitted with J. Young greaseless PTFE stopcocks using CD_2Cl_2 stored over molecular sieves and standard Schlenk line techniques to exclude moisture. Exposure to water is immediately deleterious to porphyrin polycations, but they are stable to oxygen (O_2). The neutral nanorings are only sparingly soluble in CD_2Cl_2 at low temperatures (<−40 °C), but solubility improves dramatically upon oxidation. The NMR measurements were performed on a Bruker AVII 500 spectrometer (5 mm BBFO probe). ^{1}H NMR chemical shifts were calibrated against residual proton signals of the solvent ($CHDCl_2$: $\delta_H = 5.32$ ppm), ^{13}C NMR chemical shifts were referenced to the solvent peak (CD_2Cl_2: $\delta_C = 54.00$ ppm) and ^{19}F NMR spectra were referenced to hexafluorobenzene ($\delta_F = -164.8$ ppm). At the end of each titration, decamethylferrocene was added to reduce the porphyrin nanoring back to its neutral form; the whole oxidation process is highly reversible.

Online content

Any Nature Research reporting summaries, source data, extended data, supplementary information, acknowledgements, peer review information; details of author contributions and competing interests; and statements of data and code availability are available at [https://doi.org/10.1038/s41557-019-0398-3].

Received: 26 June 2019; Accepted: 20 November 2019;
Published online: 20 January 2020

References

1. Heckmann, A. & Lambert, C. Organic mixed-valence compounds: a playground for electrons and holes. *Angew. Chem. Int. Ed.* **51**, 326–392 (2012).
2. Tolbert, L. M. & Zhao, X. Beyond the cyanine limit: Peierls distortion and symmetry collapse in a polymethine dye. *J. Am. Chem. Soc.* **119**, 3253–3258 (1997).
3. Gieseking, R. L., Ravva, M. K., Coropceanu, V. & Brédas, J.-L. Benchmarking density functional theory approaches for the description of symmetry breaking in long polymethine dyes. *J. Phys. Chem. C* **120**, 9975–9984 (2016).
4. Lorke, A. et al. Spectroscopy of nanoscopic semiconductor rings. *Phys. Rev. Lett.* **84**, 2223–2226 (2000).
5. Spitler, E. L., Johnson, C. A. II & Haley, M. M. Renaissance of annulene chemistry. *Chem. Rev.* **106**, 5344–5386 (2006).
6. Soya, T., Kim, W., Kim, D. & Osuka, A. Stable [48]-, [50]-, and [52] dodecaphyrins(1.1.0.1.1.0.1.1.0.1.1.0): the largest Hückel aromatic molecules. *Chem. Eur. J.* **21**, 8341–8346 (2015).
7. Yoneda, T., Soya, T., Neya, S. & Osuka, A. [62]Tetradecaphyrin and its mono- and bis-Zn^{II} complexes. *Chem. Eur. J.* **22**, 14518–14522 (2016).
8. Peeks, M. D., Claridge, T. D. W. & Anderson, H. L. Aromatic and antiaromatic ring currents in a molecular nanoring. *Nature* **541**, 200–203 (2017).
9. Lu, X. et al. Fluorenyl based macrocyclic polyradicaloids. *J. Am. Chem. Soc.* **139**, 13173–13183 (2017).
10. Cha, W.-Y. et al. Bicyclic Baird-type aromaticity. *Nat. Chem.* **9**, 1243–1248 (2017).
11. Lu, X. et al. Global aromaticity in macrocyclic cyclopenta-fused tetraphenanthrenylene tetraradicaloid and its charged species. *Angew. Chem. Int. Ed.* **57**, 13052–13056 (2018).
12. Gregolińska, H. et al. Fully conjugated [4]chrysaorene. Redox-coupled anion binding in a tetraradicaloid macrocycle. *J. Am. Chem. Soc.* **140**, 14474–14480 (2018).
13. Ke, X.-S. et al. Three-dimensional fully conjugated carbaporphyrin cage. *J. Am. Chem. Soc.* **140**, 16455–16459 (2018).
14. Soya, T., Mori, H. & Osuka, A. Quadruply twisted Hückel-aromatic dodecaphyrin. *Angew. Chem. Int. Ed.* **57**, 15882–15886 (2018).
15. Li, G. et al. From open-shell singlet diradicaloid to closed-shell global antiaromatic macrocycles. *Angew. Chem. Int. Ed.* **57**, 7166–7170 (2018).
16. Liu, C. et al. Macrocyclic polyradicaloids with unusual super-ring structure and global aromaticity. *Chem* **4**, 1586–1595 (2018).
17. Peeks, M. D., Jirasek, M., Claridge, T. D. W. & Anderson, H. L. Global aromaticity and antiaromaticity in porphyrin nanoring anions. *Angew. Chem. Int. Ed.* **58**, 15717–15720 (2019).
18. Peeks, M. D. et al. Aromaticity and antiaromaticity in the excited states of porphyrin nanorings. *J. Phys. Chem. Lett.* **10**, 2017–2022 (2019).
19. Fokin, A. A., Jiao, H. & v. R. Schleyer, P. From dodecahedrapentaene to the "[*n*]trannulenes". A new in-plane aromatic family. *J. Am. Chem. Soc.* **120**, 9364–9365 (1998).
20. Burley, G. A. Trannulenes with "in-plane" aromaticity: candidates for harvesting light energy. *Angew. Chem. Int. Ed.* **44**, 3176–3178 (2005).
21. Rickhaus, M. et al. Single-acetylene linked porphyrin nanorings. *J. Am. Chem. Soc.* **139**, 16502–16505 (2017).
22. Haver, R. et al. Tuning the circumference of six-porphyrin nanorings. *J. Am. Chem. Soc.* **141**, 7965–7971 (2019).
23. Gershoni-Poranne, R. & Stanger, A. Magnetic criteria of aromaticity. *Chem. Soc. Rev.* **44**, 6597–6615 (2015).
24. Chen, Z., Wannere, C. S., Corminboeuf, C., Puchta, R. & v. R. Schleyer, P. Nucleus-independent chemical shifts (NICS) as an aromaticity criterion. *Chem. Rev.* **105**, 3842–3888 (2005).
25. Stephens, P. J., Devlin, F. J., Chabalowski, C. F. & Frisch, M. J. Ab initio calculation of vibrational absorption and circular dichroism spectra using density functional force fields. *J. Phys. Chem.* **98**, 11623–11627 (1994).
26. Henderson, T. M., Izmaylov, A. F., Scalmani, G. & Scuseria, G. E. Can short-range hybrids describe long-range-dependent properties? *J. Chem. Phys.* **131**, 044108 (2009).
27. O'Sullivan, M. C. et al. Vernier templating and synthesis of a 12-porphyrin nano-ring. *Nature* **469**, 72–75 (2011).
28. Herges, R. Topology in chemistry: designing Möbius molecules. *Chem. Rev.* **106**, 4820–4842 (2006).
29. Stepien, M., Sprutta, N. & Latos-Grazynski, L. Figure eights, Möbius bands, and more: conformation and aromaticity of porphyrinoids. *Angew. Chem. Int. Ed.* **50**, 4288–4340 (2011).
30. Wirz, L. N., Dimitrova, M., Fliegel, H. & Sundholm, D. Magnetically induced ring-current strengths in Möbius twisted annulenes. *J. Phys. Chem. Lett.* **9**, 1627–1632 (2018).
31. Senthilkumar, K. et al. Lemniscular [16]cycloparaphenylene: a radially conjugated figure-eight aromatic molecule. *J. Am. Chem. Soc.* **141**, 7421–7427 (2019).
32. Fuller, F. B. The writhing number of a space curve. *Proc. Natl Acad. Sci. USA* **68**, 815–819 (1971).
33. Rappaport, S. M. & Rzepa, H. S. Intrinsically chiral aromaticity. Rules incorporating linking number, twist, and writhe for higher-twist Möbius annulenes. *J. Am. Chem. Soc.* **130**, 7613–7619 (2008).
34. Schaller, G. R. & Herges, R. Möbius molecules with twists and writhes. *Chem. Commun.* **49**, 1254–1260 (2013).
35. Kondratuk, D. V. et al. Vernier-templated synthesis, crystal structure, and supramolecular chemistry of a 12-porphyrin nanoring. *Chem. Eur. J.* **20**, 12826–12834 (2014).
36. Edwards, P. P., Lodge, M. T. J., Hensel, F. & Redmer, R. A metal conducts and a non-metal doesn't. *Phil. Trans. R. Soc. A* **368**, 941–965 (2010).
37. Hückel, E. Quantentheoretische Beiträge zum Benzolproblem I. Die Elektronenkonfiguration des Benzols und verwandter Verbindungen. *Z. Phys.* **70**, 204–286 (1931).

Data availability

All relevant data, including raw computational data from the NICS calculations as well as XYZ coordinates of calculated molecular geometries, are available within the paper and its Supplementary Information files. The NMR data are presented in detail in the main Supplementary Information file and are available upon reasonable request from the authors.

Acknowledgements

We thank the EPSRC (grants EP/N017188/1, EP/R029229/1 and EP/M016110/1), the ERC (grant 320969), the European Union's Horizon 2020 research and innovation programme (Marie Sklodowska-Curie grant SYNCHRONICS 643238) and the Swiss National Science Foundation (P300P2_174294) for funding, the National Mass Spectrometry Facility at Swansea University for MALDI mass spectra, the University of Oxford Advanced Research Computing Service (https://doi.org/10.5281/zenodo.22558) and the Australian-government-supported National Computational Infrastructure (NCI) for the provision of high-performance computing. M.J. thanks Oxford University for a Scatcherd European Scholarship. H.G. thanks the Carlsberg Foundation for a Carlsberg Foundation Internationalisation Fellowship.

Author contributions

M.R., M.J., L.T., H.G., M.D.P., R.H. and H.-W.J. synthesized the compounds; M.R. and M.J. collected and analysed the NMR spectroscopic data; M.J. and M.D.P. performed the DFT calculations; T.D.W.C. assisted with NMR data collection and interpretation; H.L.A., M.R. and M.J. devised the project and wrote the paper; all authors discussed the results and edited the manuscript.

Competing interests

The authors declare no competing interests.

Additional information

Supplementary information is available for this paper at https://doi.org/10.1038/s41557-019-0398-3.

Correspondence and requests for materials should be addressed to H.L.A.